Published in final edited form as:
*Bone*. 2014 July ; 64: 57–64. doi:10.1016/j.bone.2014.03.045.

# The Resistance of Cortical Bone Tissue to Failure under Cyclic Loading is Reduced with Alendronate

**Devendra Bajaj, Ph.D.**[a,1], **Joseph R. Geissler, M.S.E.**[a,b,1], **Matthew R. Allen, Ph.D**[c], **David B. Burr, Ph.D.**[c], and **J. Christopher Fritton, Ph.D.**[a,b]

Devendra Bajaj: devendrabajaj@gmail.com; Joseph R. Geissler: geissljr@rutgers.edu; Matthew R. Allen: matallen@iupui.edu; David B. Burr: dburr@iupui.edu; J. Christopher Fritton: chris.fritton@rutgers.edu

[a]Department of Orthopaedics, New Jersey Medical School, Rutgers University, 205 S. Orange Avenue, Newark, NJ 07103, USA

[b]Department of Biomedical Engineering, New Jersey Institute of Technology, 323 Martin Luther King, Jr. Boulevard, Newark, NJ 07102, USA

[c]Department of Anatomy and Cell Biology, Indiana University School of Medicine, 635 Barnhill Drive, Indianapolis, IN 46202, USA

## Abstract

Bisphosphonates are the most prescribed preventative treatment for osteoporosis. However, their long-term use has recently been associated with atypical fractures of cortical bone in patients who present with low-energy induced breaks of unclear pathophysiology. The effects of bisphosphonates on the mechanical properties of cortical bone have been exclusively studied under simple, monotonic, quasi-static loading. This study examined the cyclic fatigue properties of bisphosphonate-treated cortical bone at a level in which tissue damage initiates and is accumulated prior to frank fracture in low-energy situations. Physiologically relevant, dynamic, 4-point bending applied to beams (1.5 mm × 0.5 mm × 10 mm) machined from dog rib (n=12/group) demonstrated mechanical failure and micro-architectural features that were dependent on drug dose (3 groups: 0, 0.2, 1.0 mg/kg/day; Alendronate [ALN] for 3 years) with cortical bone tissue elastic modulus (initial cycles of loading) reduced by 21% ($p<0.001$) and fatigue life (number of cycles to failure) reduced in a stress-life approach by greater than 3-fold with ALN1.0 ($p<0.05$). While not affecting the number of osteons, ALN treatment reduced other features associated with bone remodeling, such as the size of osteons (−14%, ALN1.0: 10.5±1.8, VEH: 12.2±1.6, $\times 10^3$ $\mu m^2$; $p<0.01$) and the density of osteocyte lacunae (−20%; ALN1.0: 11.4±3.3, VEH: 14.3±3.6, $\times 10^2$ #/$mm^2$; $p<0.05$). Furthermore, the osteocyte lacunar density was directly proportional to initial elastic modulus when the groups were pooled ($R=0.54$, $p<0.01$). These findings suggest that the structural components normally contributing to healthy cortical bone tissue are altered by high-



**Address for correspondence**: J. Christopher Fritton, Ph.D., Department of Orthopaedics, Rutgers, the State University of NJ, NJ Medical School, Cancer Center, G-1216, 205 South Orange Avenue, Newark, NJ 07103, USA, Phone: (973) 972-2595, Fax: (973) 972-1875, chris.fritton@rutgers.edu.
[1]These authors contributed equally.

dose ALN treatment and contribute to reduced mechanical properties under cyclic loading conditions.

**Keywords**

bone remodeling; osteocytes; atypical fracture; antiresorptives; osteoporosis

## 1 Introduction

**B**isphosphonates, including oral alendronate developed by Merck (Fosamax) and now available in generic form, are bone anti-resorptive drugs. As the most commonly prescribed treatment for the prevention of osteoporotic fracture, over 5 million U.S. patients filled a prescription for an oral bisphosphonate in each year from 2005 to 2009, the last year in which reliable data are available.[1] By suppressing resorption, bisphosphonates slow the loss of bone mass at the hip and spine.[2] Consequently, fracture risk at these highly trabecular skeletal sites is reduced.[3–7] However, long-term suppression of bone resorption and remodeling also affects the quality of bone by altering tissue-level micro-architecture and composition.[8–10] Notably, in iliac crest patient biopsies, bisphosphonate treatment was shown to slow the loss of trabecular micro-architecture, quantified as number, thickness and interconnectedness of plate-like and rod-like elements.[2, 11] In these same biopsies, [12] and in dogs (vertebrae and tibia) treated with anti-resorptives,[13, 14] cortical bone micro-architecture and composition have demonstrated more tissue damage and mineral crystal homogeneity, two components of bone's mechanical quality.

Alterations in quality can also impact cortical bone's fracture resistance. Indeed, several studies on the mechanical behavior of short-term (1 year) and long-term (3 years) bisphosphonate-treated bones (ilium, ribs, spinous processes and vertebrae) from dogs, a species exhibiting intra-cortical resorption patterns similar to human, have shown increased stiffness, or initial resistance to a mechanical load, yet decreased toughness, or energy absorption to fracture, as estimated from whole-bone mechanical testing.[8, 13, 15–18] More direct tests at the tissue level on machined specimens from tibia of bisphosphonate-treated animals and iliac crest biopsies from treated patients have also suggested lower toughness by traditional bone beam bending,[19] and "plastic deformation resistance" by nanoindentation (a non-traditional surrogate),[20] which are both generally associated with increased brittleness.

While remodeling suppression with bisphosphonates is associated with changes in material properties determined from these quasi-static mechanical tests in which failure occurs in a single loading cycle, properties of the tissue under more realistic, cyclic (fatigue) loading conditions are unknown. *In vivo*, bones are naturally loaded cyclically. This repetitive loading results in initiation of micro-damage that is normally repaired by targeted remodeling, the process of bone tissue renewal.[21, 22] Bone tissue aging is associated with brittleness,[13, 17] and one plausible explanation for the recently described association of atypical cortical shaft fractures occurring after long-term (>3–5 years) bisphosphonate treatment[1, 23–30] is that by slowing targeted bone tissue repair, micro-damage

accumulates, eventually resulting in a frank fracture. While the mechanisms have not been elucidated, studies on non-treated bone from many species have demonstrated that fatigue-induced micro-damage accumulation compromises mechanical integrity.[31–35] Further, in a well-controlled dog model, increases in the average length of micro-cracks with bisphosphonate treatment versus saline control were evident within cortical bone after three years.[8, 17] This aspect of micro-damage, and no other, including the density of cracks (#/mm$^2$), has been found altered in cortical bone of dog rib only with bisphosphonate treatment.

The current study evaluated the cyclic fatigue behavior of cortical bone from dogs that had been treated for three years with two clinically relevant doses of oral alendronate. A conventional engineering fatigue-life approach was utilized to determine whether the number of cycles to failure is a function of alendronate treatment. The hypotheses tested were that long-term bisphosphonate treatment impairs the fatigue-life and tissue-level properties of cortical bone, and does so in a dose-dependent manner. Observations were also made of trabecular and cortical tissue micro-architecture, the osteons and embedded cell lacunae.

## 2 Materials and Methods

### 2.1 Animal Model

36 adult female beagles (1–2 years old) were purchased from LBL (Reelsville, IN). On arrival, lateral thoracic x-rays of all dogs were obtained under anesthesia (Pentothal, 10 mg/kg, intravenous, Abbott Laboratories, Chicago, IL), to confirm skeletal maturity (closed proximal tibia and lumbar vertebral growth plates). Animals were housed 2 per cage in environmentally controlled rooms and fed standard dog chow containing 1.2% calcium, 1.0% phosphorus, and 850 IU/kg vitamin D3 (Diamond Premium Adult, Diamond Pet Foods, Meta, MO). Water was available at all times. After 2 weeks of acclimatization, dogs were assigned to the 3 equal-sized treatment groups based on matched body masses. Groups were treated daily with an oral dose of vehicle (VEH, 1mL/kg saline) or Alendronate (ALN, 0.2 mg/kg or 1.0 mg/kg; Merck) for 3 years.[8] Alendronate was dissolved in saline as either a 0.05% solution (0.2 mg dose) or a 0.2% solution (1.0 mg dose) with a correction for the 16.4% moisture content. Alendronate doses were chosen to correspond to doses used clinically for the treatment of postmenopausal osteoporosis and Paget's disease, respectively. Appropriate amounts of the alendronate solution were supplemented with saline to reach a total volume of 10 mL for each daily dose. Doses were administered with a syringe each morning after an overnight fast and at least 2 hours before feeding. No dogs were lost prior to euthanasia and all appeared healthy. Animals were euthanized by intravenous administration of sodium pentobarbital (0.22 mg/kg Beuthanasia-D Special). After death, right 10$^{th}$ and 11$^{th}$ ribs were excised and stored frozen (−20°C) in saline soaked gauze. All procedures were approved by the Indiana University School of Medicine Animal Care and Use Committee. Each measurement was made by one observer blinded to treatments received in each group.

### 2.2 Biomechanical Fatigue Testing

Data for bones from these dogs have been presented previously.[8, 13] However, data presented here are for cyclically loaded rib bone. This bone was fresh frozen immediately after euthanasia and was stored for two years prior to machining for testing. Beams were prepared from medial and lateral $11^{th}$ rib cortices using slicing equipment (Buehler Isomet 5000, Barranca Diamond-303 Professional 102 mm × 360 μm diamond-coated lapidary blade). A slow speed (2500 rpm, 3.0 mm/min feed rate) was used to minimize machining marks and no additional polishing was done. First, each rib was cut into 4 approximately equal length sections (Figure 1a). These sections were potted in quick setting resin cement (Bondo) and a 1.5 mm primary section was made along the medio-lateral axis. Secondary sections were introduced in the medial and lateral cortex to obtain beams of rectangular cross-sectional geometry (1.5 mm × 0.5 mm) and 10–12 mm length (Figure 1b). In this configuration, the long-axis of osteons is oriented parallel to the beam length. The uniform rectangular geometry was maintained equivalent for each beam (VEH: 1.57±0.11 mm × 0.48±0.04 mm; ALN0.2: 1.51±0.05 mm × 0.50±0.05 mm; ALN1.0: 1.54±0.10 mm × 0.52±0.06 mm). The strict geometrical adherence forced the number of beams prepared from each rib to vary due to bone curvature. A total of 92 beams were prepared (1–5 beams per rib).

For mechanical testing, beams were centered in a 4-point loading fixture with the periosteal side in tension and the endosteal side in compression. The outer and inner supports were set 6 mm and 2 mm apart, respectively. All tests were conducted at room temperature in a controlled lab environment with the specimen submerged in a saline bath (Sigma Buffered Saline with $PO_4$, $MgCl_2$ and $CaCl_2$, D86622).[32] Cyclic loads were applied sinusoidally at a stress ratio ($R = \sigma_{min}/\sigma_{max}$) of 0.1 (Figure 1c) and frequency of 2 cycles per second (Hz), under load control by an electro-mechanical actuator (Bose Testbench). Fatigue loads were applied with stress amplitudes ($\sigma_a = ½[\sigma_{max} - \sigma_{min}]$) ranging from 45–85 MPa.

Beams obtained from the same rib were tested at different stress amplitudes. Thus, fatigue response at any given stress amplitude was comprised of beams from several ribs. Beams were tested until failure or a pre-defined number of cycles (N=250,000). Failure was defined by either fracture of beam or a 2.5 mm total deflection, whichever occurred first. The rationale for the deflection failure limit was that in our preliminary work, beams that had not attained catastrophic failure had entered into the tertiary phase of, but were not progressing toward, failure. The load vs. load-line displacement data was recorded at 100 Hz and was used to calculate the stress ($\sigma$) and strain ($\varepsilon$) according to conventional beam theory. Secant modulus (E) in a given cycle, defined as the slope of the line connecting the 2 points, $\sigma_{max}$, $\varepsilon_{max}$ and $\sigma_{min}$, $\varepsilon_{min}$ (Figure 1c), was monitored throughout the test and plotted after test completion at specific fractions of the total fatigue life.[36]

Loss of modulus ($\Delta E$) over the fatigue life was calculated by subtracting the final $E_f$ just prior to failure (1 cycle) from the initial $E_i$ (during the 10th cycle). All specimens self-adjusted in the loading fixtures within 10 cycles to achieve the prescribed $\sigma_a$. Fatigue life was modeled using a power law for both $\sigma_a$ and $\varepsilon$ so that $\sigma_a = A(N_f)^B$ and $\varepsilon = A(N_f)^B$, where $N_f$ is the number of cycles to failure, and A and B are coefficient and exponent, respectively.

All mechanical parameters, including moduli and cycles to failure, were observed to be site specific with differences of 25 – 50% ($p<0.05$) between beams machined from different cortices (Tables S1 and S2). This was ascribed to differences in porosity, where highly porous beam specimens of the lateral cortex had individual osteonal average canal area (Ca.Ar) measured by histomorphometry that exceeded the size of any canal found medially and total Ca.Ar that exceeded 3% of total beam cross-sectional area. The geometrical constraints of the rib cortices did not allow production of enough lateral beams for a complete statistical analysis. Therefore, data presented in the main text are from medial beams with data from no fewer than 2 dogs per group represented at each stress level. Data from both cortices are reported in supplemental results.

### 2.3 Histomorphometry

After mechanical testing, beams were bulk stained in 1% basic fuchsin and embedded in polymethyl-methacrylate using standard staining and embedding protocols.[8, 16, 22, 37] The plastic blocks were then cut to obtain 300 μm thick sections, transverse to the beam length. Sections were ground to 100 μm thickness and fine polished with alumina slurries (successive particle diameters of 1.0 and 0.05 μm) on a cloth wheel (Buehler Isomet). Bone beam cross sections were imaged under a bright field microscope (Eclipse 50i, Nikon) at 10× magnification and stitched together using a graphics editing program (Adobe Photoshop CS5). For each bone beam, 3–5 cross sections from the mid-span were imaged. Osteon cement lines and Haversian canals were traced, and osteocyte lacunae point counted on the digital images with an interactive pen/tablet desktop workstation (Wacom Cintiq 21UX). Thus, cross sections were analyzed for micro-architectural parameters, including canal porosity (average canal area, Ca.Ar; canal density, Ca.Dn), osteonal composition (average osteon area, On.Ar; osteon density, On.Dn), and osteocyte lacunae density (Ot.Lc.Dn) in each of the three compartments, osteonal, interstitial and combined total beam cross-sectional area.[38]

### 2.4 μCT

Randomly selected $10^{th}$ ribs (n=6/group) were evaluated by micro-computed tomography (SkyScan 1172 μCT; 80keV, 126μA) for density and morphology. Ribs were submerged in saline and scanned, two at a time, at an isotropic voxel resolution of 17 μm. Density calibration phantoms (0.25 and 0.75 g/cm$^3$) were also scanned to enable cortical (Ct) tissue mineral density calculations (TMD). Cortical and trabecular traits were measured in an 8 mm length of the midspan of each rib [average cortical width (Ct.Wi), cortical bone area (Ct.Ar), medullary (or marrow) area (Ma.Ar) and Ct.Ar normalized by total area within the periosteal envelope (Ct.Ar/Tt.Ar); trabecular thickness (Tb.Th), separation (Tb.Sp), number (Tb.N), pattern factor (Tb.Pf), area (Tb.Ar) and bone mineral density (Tb.BMD)].

### 2.5 Analysis of Data

To investigate variance between treatment groups, most data sets were analyzed using analysis of variance (ANOVA). Analysis of covariance (ANCOVA) was utilized to assess differences between groups in fatigue life and examine possible relationships between Ot.Lc.Dn and $E_i$. Post-hoc analysis was completed with Tukey HSD for multiple comparisons (Matlab Statistics Toolbox). Normality of data sets was determined with

Shapiro-Wilk's Test.[39] Statistical significance is reported at $p<0.05$, unless otherwise noted.

## 3 Results

### 3.1 Mineral Density and Structure from Whole Ribs

ALN treatment did not affect rib Ct.TMD (Table 1) based on X-ray absorption as measured by μCT. Cortical bone structure reflected effects of modified resorption in that the average cross-sectional Ct.Ar/Tt.Ar was significantly ($p<0.05$) greater with drug treatment versus VEH (ALN0.2: +9%; ALN1.0: +13%). This was attributed to greater amounts of bone at the endosteal surfaces as evidenced by significantly ($p<0.05$) smaller Ma.Ar compared to VEH (ALN0.2: – 20%; ALN1.0: −25%). The average cross-sectional area fraction occupied by trabecular bone (Tb.Ar/Ma.Ar) was also significantly ($p<0.05$) greater with ALN1.0 (+34%) versus VEH treatment (Table S3). This was attributed to a significant ($p<0.05$) decrease (−34%) in the average separation (Tb.Sp) between the plate-like trabeculae.

### 3.2 Biomechanical Fatigue Testing

Cyclic mechanical loads imposed on cortical bone beams exposed differences in mechanical properties of treated tissues. Modulus loss was observed as cycle number increased and exhibited the typical 3-phase response in all specimens (Figure S1). Average modulus of the initial loading cycle, $E_i$, and just prior to the final loading cycle, $E_f$, were significantly lower for ALN1.0 treatment compared to VEH by 21% ($p<0.001$) and 30% ($p<0.01$), respectively (Figure 2a). $E_i$ was also significantly lower for ALN1.0 compared to ALN0.2 by 15% ($p<0.01$). No significant differences were found for $E_i$ or $E_f$ between ALN0.2 and VEH ($p>0.16$), $E_f$ between ALN1.0 and ALN0.2 ($p>0.80$), or $\Delta E$ between any treatment group ($p>0.25$). ALN treatment resulted in a reduction of the fatigue life of cortical bone (Figure 3) as the $\sigma_a$ power-law fit for the ALN1.0 group revealed that these bones took 3-fold fewer cycles to fail compared to those from VEH ($p<0.05$). No significant differences were found between ALN0.2 and either ALN1.0 or VEH, though a trend for dose effects was indicated by ANCOVA ($p<0.01$). While a significant p-value was indicated for the effect of cycles on apparent strain ($\varepsilon$) amplitude, the Tukey HSD on the power-law fit models did not reach significance ($p>0.14$) for any difference between groups (Figure 3).

### 3. 3 Cortical Micro-architecture

The micro-architecture of cortical osteonal bone consists of 3 main features: osteons, osteonal canals and the interstitial space between the osteons. Morphometry of stained histological cross sections revealed that osteonal area in beams from the ALN1.0 treated group was significantly ($p<0.01$) smaller than VEH (Figure 4a,b). Since the density of osteons did not differ between treatments, the average osteon area was 14% smaller ($p<0.01$) for ALN1.0 compared to VEH. No differences ($p>0.15$) were observed between ALN0.2 and the other groups in osteon area. Osteonal canal size was not different ($p>0.15$) between any of the 3 groups, with all groups exhibiting average Ca.Ar below 2.5% (Table 2).

### 3.4 Osteocyte Lacunae Density

The cell population in cortical bone tissue is predominantly composed of osteocytes, each one positioned within a single lacuna in the osteonal or interstitial areas. Morphometry of the cortical beam cross sections revealed that osteocyte lacunae density (Ot.Lc.Dn) within osteons from both the ALN0.2 ($p<0.01$) and ALN1.0 ($p<0.05$) treated groups was at least 20% lower than in VEH (Figure 4c). Ot.Lc.Dn of the interstitial spaces was not significantly different than that within osteons for each group and was similarly lower for drug-treated groups (ALN0.2: 1059±273; ALN1.0: 1141±378, vs. VEH: 1343±301). Thus, the overall total Ot.Lc.Dn followed the same trend of 20% reduction ($p<0.05$) for ALN versus VEH-treated bone. Examination of the relationships between mechanical properties and Ot.Lc.Dn revealed that a moderately strong correlation ($R=0.54$) existed such that greater $E_i$ implied greater Ot.Lc.Dn when data from the groups were pooled together. No differences between groups were found in the linear regression models (Figure 5).

## 4 Discussion

Long-term (3-year) treatment with high-dose ALN has adverse effects on the mechanical behavior of cyclically loaded cortical bone tissue. These new findings have implications for atypical fracture risk and occurred despite the benefit that this drug has for trabecular micro-architecture in highly remodeled areas of the skeleton, as was reinforced in the current study.[2, 14, 18] Not surprisingly, the trabecular data for ALN-treated, aging female beagles (Table S3) reflect that clinical use of bisphosphonates maintains bone in trabecular regions and reduces fracture risk.[1, 3–7] Conversely, the long-term effects of bisphosphonates on cortical bone have recently come under greater scrutiny by the research community and the FDA due to reports of rare but serious types of atypical fracture.[1, 23–30] Though the mechanisms require further elucidation, one distinct difference with bisphosphonate versus vehicle treatment in the dog model is greater length of micro-cracks in cortical bone.[8, 17] This may be indicative of incomplete removal of damage in high-dose treatment that contributes to the reduced mechanical properties as determined in this study.

Both bone tissue damage and the osteonal bone remodeling that removes damage are important to bone tissue quality. The damage process dissipates energy during daily cyclic loading events.[40] From an engineering point of view, repair must keep pace with damage growth in order to leave the structure intact as appears to be the case for low-dose treatment in this beagle model. However, greater damage in the form of 25% longer micro-crack length demonstrated after both 1 and 3 years on the high-dose ALN suggested a reduction in tissue-level toughness, or the amount of energy required to fracture whole ribs under simple, mono-tonic, quasi-static mechanical loading.[8, 17] Because bone structure is preserved or even enhanced with ALN treatment as confirmed in the present study for both low and high doses compared to VEH (Table 1), the apparent-level tissue toughness was previously estimated from whole-bone tests. Elucidating the possible mechanisms behind this estimated loss in toughness helped motivate the current study, and separating the effects from those due to whole-bone geometry required machining prismatic beams. Furthermore, the quasi-static loading used previously did not allow for the study of damage processes within the tissue as relatively little time is available for the development of damage, i.e., quasi-static

mechanical tests to failure typically take no more than minutes to complete, while many of the cyclic fatigue tests completed for this study took longer than a day.

More completely capturing one aspect of the complex nature of *in vivo* cyclic mechanical loading by performing fatigue bending has revealed a possible mechanical mechanism behind the weakening and atypical fracture of cortical bone tissue with long-term bisphosphonate treatment. Proposed contributors to the atypical fracture side-effect of bisphosphonates are also consequences of reduced remodeling and include increased tissue age, homogeneity, mineralization and accumulation of non-enzymatic glycation products.[9, 11, 12, 13, 19, 40] These may all contribute to the tissue-level mechanical properties previously found. For example, nanoindentation for hardness demonstrated increased tissue modulus in trabeculae of iliac crest biopsies of patients with lower bone turnover due to bisphosphonate treatment.[10, 41] No difference was found in the biopsy cortical shell. This may seem to contradict what was found in the current study, lower $E_i$ with ALN treatment. However, the apparent-level bending test performed here, as opposed to the tissue-level nanoindentation test, is more likely to drive existing damage toward propagation and accumulation. Thus, the most probable mechanical explanation for the findings of reduced modulus (E, Figure 2a) and number of cycles to failure (Figure 3) in the current study is greater micro-crack burden in the form of greater crack length in the high-dose ALN treatment group.[8] Relatively low $E_i$ in 4-point bending might even occur for a hard, brittle material with high average E as measured by nanoindentation, for example, when inclusions such as pores and/or differentially mineralized regions are present.

Large, long-lived adult animals, such as dogs and humans, exhibit micro-damage that is remodeled away by basic multicellular units (BMUs) that are absent from mice and rats.[42, 43] The resulting osteons have interfaces with the old interstitial bone, the cement lines (Figure 6), which are tough and resist micro-crack propagation.[44–46] Furthermore, during the remodeling process each osteon is embedded with multiple networked sensors, the long-lived osteocytes, capable of detecting damage and relaying remodeling activation signals to target BMUs to damaged areas when required. The density of osteocytes in an osteon is greatest at the cement line, which represents the reversal of a BMU from resorption to formation by osteoblasts, and therefore, the first newly differentiated osteocytes.[47] That osteocyte density is greatest at an interface, where damage eventually propagates to and accumulates at, is compatible with the role of osteocytes as damage sensors. The relationship between osteocyte lacunae density within osteons and $E_i$ (Figure 5) may indicate impaired detection of damage at the cement line or within the rest of the tissue. This does not prove that osteocyte density determines mechanical properties at the tissue level. However, osteocyte deficiency has been associated with osteoporotic fracture and could contribute to bone fragility through this damage detection mechanism.[48] For example, reduced osteon size and reduced osteocyte density within osteons may result in a combination that allows interstitial damage dissociation from an area where normally detected, the cement line (Figure 6).

While the outer ring represents the oldest tissue of the osteon, much older tissue resides in the interstitial space on the other side of most cement lines. A consequence of smaller osteons in the high-dose ALN group (Figure 4a) is that the amount of interstitial cortical

bone increases (Figure 6). In this older tissue more damage tends to accumulate.[49, 50] That accumulation has at least two possible explanations. First, the tissue may be more easily damaged due to biochemical or ultra-structural differences such as greater accumulation of advanced glycation end-products or higher mineralization.[51, 52] Second, there may be slower removal and replacement of damaged tissue. At this point only speculations exist that sites of atypical fracture contain older tissue and that microdamage accumulates more quickly following a long-term bisphosphonate treatment. Little damage data has been collected from sites of atypical fracture or from iliac crest biopsies of atypical fracture patients as was recently reviewed.[53]

Because intracortical BMUs must originate at a blood vessel, generally located in the middle of an osteon (Figures 4b, 6), removal of interstitial tissue requires either greater activation of BMUs to place new blood vessels in proximity to the older, damaged tissue or deeper digging by osteoclasts. Both the activation frequency for new BMUs and the width of resorption cavities are reduced with ALN in this dog model, yet osteons do turn over and the density of osteons is not affected (Figure 4a).[8, 14, 17, 51] Based on these measures, approximately 60% of osteons had their micro-architecture affected over the 3 years of high-dose ALN treatment, assuming that activation did not occur in the same spatial location multiple times.[8, 16] The reduction in average osteon cross-sectional size is most likely attributable to a reduced width (25%) of BMU resorption cavities as measured in trabecular bone of this dog model with high-dose treatment.[54]

Although we planned and standardized protocols to avoid differences in testing that would differentially affect the three groups, limitations exist in this study that was designed primarily to examine the effects on bone tissue mechanical properties after a continuous term of three-year ALN treatment. First, the time component of fatigue loading allows for creep to occur, and resulting large deformations could have contributed to the failure of samples. Greater numbers of beams in the drug-treated groups than control reached our pre-defined deformation failure criterion (Table S1). Second, a longer duration of dosing might be expected to result in a greater reduction in number of cycles to failure. This may be important to determine because the duration of clinical bisphosphonate treatment has been positively associated with greater atypical fracture risk in the only large, long-term prospective report to date that included patients out to a maximum of 13 years of drug treatment.[30] Increased risk of atypical fracture appears to occur at mean and median bisphosphonate treatment durations of 5 and 7 years in patients.[28, 30] Cortical tissue replacement periods for dogs of 2+ months are approximately half that for humans, based on the calculated human remodeling period of 4 – 6 months.[54–56] Thus, the current 3-year study may be considered time-equivalent to 6 years of treatment in the human and when effects on fatigue life might be observed. However, whether the differences found in this study would exist with other durations of treatment or in an established osteoporotic model is unknown. A third limitation was that bending loads were applied sinusoidally with a single frequency, and in a single anatomical plane, perpendicular to the long axis of the osteons (Figure 1b). One of the primary limitations of 4-point bending is that strain ($\varepsilon$) fields in the nonhomogenous cortical bone tissue beams are likely complex and affected by the microstructural differences found in the groups. One simplified model for apparent strain ($\varepsilon$) did not demonstrate differences in fatigue life between the groups (Figure 3). Additionally,

physiological loads are more complex with multiple modes, directions and time components. Finally, only rib bone from the beagle was examined. The choice of rib bone versus another load-bearing bone was made to capture any effects on remodeling. While cortical rib bone of dogs and humans is not associated with weight bearing, this site undergoes greater remodeling compared to other bones due to the high frequency of loading associated with breathing. At a typical breathing rate of 30 breaths per minute (0.5 Hz) the numbers of loading cycles on dog rib tissue reaches similar values in 4× the length of time of our 2 Hz dynamic fatigue loading. However, most of those *in vivo* loading cycles will be at lower stress levels than we utilized. Because the rib bone is also relatively small, the initial intent was to include beams cut from both medial and lateral cortices. However, in the course of the study the lateral cortex was found to have very large osteonal canals (>3% of total beam area). This large porosity appears to contribute to poor mechanical properties, including a 30% lower initial modulus than in beams from the medial cortex (Table S1).

Despite the limitations, the data provide important clues on the effects of suppressing bone tissue remodeling. While post-hoc analysis indicated a significantly decreased number of cycles to failure with high-dose drug treatment only, a trend for dose effects by ANCOVA (Figure 3, $p<0.01$) and other interesting data suggest that the low-drug dose also affected bone tissue quality. While osteon size was not affected by low-dose treatment, the density of osteocyte lacunae within osteons was significantly lower, in similar fashion to the high-dose treatment (−20%). If sensor density affects the recruitment of osteoclasts, then loss in osteocyte density may portend the larger crack lengths measured in this model with high-dose treatment and loss of mechanical properties. However, whether mechanical differences at the lower dose would become more apparent with longer duration treatment is unknown.

Results from this study offer insight into the possible link between long-term bisphosphonate treatment and changes in material properties. While this investigation showed that high and low-dose ALN successfully maintained cortical tissue mineral density, results also demonstrate that high-dose ALN treatment reduces stiffness and, most importantly, fatigue life. During healthy remodeling of cortical tissue, old or damaged bone is normally replaced with new osteons of similar shape and size, maintaining the overall osteonal area (Figure 6).[42, 57] The conservation of osteon size not only maintains the amount of interstitial area where damage tends to be found, but also ensures that osteons remain in close proximity to one another, providing structural reinforcement. However, this study has demonstrated that high-dose ALN treatment results in a nearly 14% reduction in osteonal area, while conserving the total number of osteons. In addition, osteonal composition is critical for maintaining toughness, as cracks are generally stopped or deflected by interlamellar debonding inside the osteons, or by delamination at the weak osteon-matrix interface, i.e., cement line.[41, 43–46] Combined, these results suggest that the structural components normally contributing to healthy bone tissue are altered by high-dose ALN treatment and contribute to reduced mechanical properties under cyclic loading conditions.

## Supplementary Material

Refer to Web version on PubMed Central for supplementary material.

## Acknowledgments

We thank Sadiq Khan and Shahir Monsuruddin (NJIT), and Linda Uko and Edek Williams (Rutgers) for technical assistance. Alendronate was provided at no cost by Merck. This investigation utilized an animal facility constructed with support from a Research Facilities Improvement Program from the National Center for Research Resources of the National Institutes of Health (NIH award number C06 RR010601-01). Research reported in this publication was supported by the National Institute of Arthritis and Musculoskeletal and Skin Diseases of the NIH (award numbers: AR062002 to MRA, AR047838 and AR007581 to DBB, AR063351 to JCF), the National Space Biomedical Research Institute through NASA contract NCC 9-58 (Fellowship to DB), and the New Jersey Space Grant Consortium and Sigma Xi (Awards to JRG). The content is solely the responsibility of the authors and does not necessarily represent the official views of any funding agency.

**Authors' roles**: Conception and design of the study: DB, MRA, DBB and JCF. Study conduct: DB, JRG and MRA. Acquisition of data: DB and JRG. Analysis of data: DB, JRG and JCF. Interpretation of data: DB, JRG and JCF. Drafting article: DB, JRG and JCF. Revising article critically for important intellectual content: MRA, DBB and JCF. Final approval of the version submitted: DB, JRG, MRA, DBB and JCF.

## Abbreviations

| | |
|---|---|
| **ALN** | alendronate |
| **a** | amplitude |
| **Ar** | area |
| **BMU** | basic multicellular unit |
| **Ca** | canal |
| **Ct** | cortical |
| **Dn** | density |
| **E** | modulus of elasticity |
| **f** | final |
| **Hz** | Hertz |
| **i** | initial |
| **Lc** | lacunae |
| **P** | load |
| **Ma** | marrow |
| **μCT** | micro-computed tomography |
| **max** | maximum |
| **min** | minimum |
| **N** | number |
| **Ot** | osteocyte |
| **On** | osteon |
| **R** | ratio |
| **Sp** | separation |

| | |
|---|---|
| **K** | stiffness |
| **σ** | stress |
| **ε** | strain |
| **TMD** | tissue mineral density |
| **Tt** | total |
| **Tb** | trabecular |
| **VEH** | vehicle |
| **Wi** | width |

## References


1. FDA. Background Document for Meeting of Advisory Committee for Reproductive Health Drugs and Drug Safety and Risk Management Advisory Committee September 9, 2011. 2011. http://www.fda.gov/downloads/AdvisoryCommittees/CommitteesMeetingMaterials/Drugs/DrugSafetyandRiskManagementAdvisoryCommittee/UCM270958.pdf.
2. Rodan GA, Fleisch HA. Bisphosphonates: mechanisms of action. J Clin Invest. 1996; 97:2692–2696. [PubMed: 8675678]
3. Black DM, Cummings SR, Karpf DB, Cauley JA, Thompson DE, Nevitt MC, Bauer DC, Genant HK, Haskell WL, Marcus R, Ott SM, Torner JC, Quandt SA, Reiss TF, Ensrud K. Randomised trial of effect of alendronate on risk of fracture in women with existing vertebral fractures. Fracture intervention trial research group. The Lancet. 1996; 348:1535–1541.
4. Black DM, Thompson DE, Bauer DC, Ensrud K, Musliner TA, Hochberg MC, Nevitt MC, Suryawanshi S, Cummings SR. Fracture risk reduction with alendronate in women with osteoporosis: The fracture intervention trial research group. J Clin Endocrinol Metab. 2000; 85:4118–4124. [PubMed: 11095442]
5. Cummings SR, Black DM, Thompson DE, Applegate WB, Barrett-Connor E, Musliner TA, Palermo L, Prineas R, Rubin SM, Scott JC, Vogt T, Wallace R, Yates AJ, LaCroix AZ. Effect of alendronate on risk of fracture in women with low bone density but without vertebral fractures: Results from the fracture intervention trial. JAMA. 1998; 280:2077–2082. [PubMed: 9875874]
6. Liberman UA, Weiss SR, Broll J, Minne HW, Quan H, Bell NH, Rodriguez-Portales J, Downs RW, Dequeker J, Favus M. Effect of oral alendronate on bone mineral density and the incidence of fractures in postmenopausal osteoporosis. The alendronate phase III osteoporosis treatment study group. N Engl J Med. 1995; 333:1437–1443. [PubMed: 7477143]
7. Mackey DC, Black DM, Bauer DC, McCloskey EV, Eastell R, Mesenbrink P, Thompson JR, Cummings SR. Effects of antiresorptive treatment on nonvertebral fracture outcomes. J Bone Miner Res. 2011; 26:2411–2418. [PubMed: 21710615]
8. Allen MR, Reinwald S, Burr DB. Alendronate reduces bone toughness of ribs without significantly increasing microdamage accumulation in dogs following 3 years of daily treatment. Calcif Tissue Int. 2008; 82:354–360. [PubMed: 18463913]
9. Bala Y, Depalle B, Farlay D, Douillard T, Meille S, Follet H, Chapurlat R, Chevalier J, Boivin G. Bone micromechanical properties are compromised during long-term alendronate therapy independently of mineralization. J Bone Miner Res. 2012; 27:825–834. [PubMed: 22189833]
10. Boivin GY, Chavassieux PM, Santora AC, Yates J, Meunier PJ. Alendronate increases bone strength by increasing the mean degree of mineralization of bone tissue in osteoporotic women. Bone. 2000; 27:687–694. [PubMed: 11062357]
11. Roschger P, Rinnerthaler S, Yates J, Rodan GA, Fratzl P, Klaushofer K. Alendronate increases degree and uniformity of mineralization in cancellous bone and decreases the porosity in cortical bone of osteoporotic women. Bone. 2001; 29:185–191. [PubMed: 11502482]

12. Donnelly E, Meredith DS, Nguyen JT, Gladnick BP, Rebolledo BJ, Shaffer AD, Lorich DG, Lane JM, Boskey AL. Reduced cortical bone compositional heterogeneity with bisphosphonate treatment in postmenopausal women with intertrochanteric and subtrochanteric fractures. J Bone Miner Res. 2012; 27:672–678. [PubMed: 22072397]
13. Allen MR, Burr DB. Three years of alendronate treatment results in similar levels of vertebral microdamage as after one year of treatment. J Bone Miner Res. 2007; 22:1759–1765. [PubMed: 17663638]
14. Gourion-Arsiquaud S, Allen MR, Burr DB, Vashishth D, Tang SY, Boskey AL. Bisphosphonate treatment modifies canine bone mineral and matrix properties and their heterogeneity. Bone. 2010; 46:666–672. [PubMed: 19925895]
15. Allen MR, Iwata K, Phipps R, Burr DB. Alterations in canine vertebral bone turnover, microdamage accumulation, and biomechanical properties following 1-year treatment with clinical treatment doses of risedronate or alendronate. Bone. 2006; 39:872–879. [PubMed: 16765660]
16. Komatsubara S, Mori S, Mashiba T, Li J, Nonaka K, Kaji Y, Akiyama T, Miyamoto K, Cao Y, Kawanishi J, Norimatsu H. Suppressed bone turnover by long-term bisphosphonate treatment accumulates microdamage but maintains intrinsic material properties in cortical bone of dog rib. J Bone Miner Res. 2004; 19:999–1005. [PubMed: 15125797]
17. Mashiba T, Hirano T, Turner CH, Forwood MR, Johnston CC, Burr DB. Suppressed bone turnover by bisphosphonates increases microdamage accumulation and reduces some biomechanical properties in dog rib. J Bone Miner Res. 2000; 15:613–620. [PubMed: 10780852]
18. Mashiba T, Turner CH, Hirano T, Forwood MR, Jacob DS, Johnston CC, Burr DB. Effects of suppressed bone turnover by bisphosphonates on microdamage accumulation and biomechanical properties in clinically relevant skeletal sites in beagles. Bone. 2001; 28:524–531. [PubMed: 11344052]
19. Tang SY, Allen MR, Phipps R, Burr DB, Vashishth D. Changes in non-enzymatic glycation and its association with altered mechanical properties following 1-year treatment with risedronate or alendronate. Osteoporos Int. 2009; 20:887–894. [PubMed: 18850239]
20. Tjhia CK, Stover SM, Rao DS, Odvina CV, Fyhrie DP. Relating micromechanical properties and mineral densities in severely suppressed bone turnover patients, osteoporotic patients, and normal subjects. Bone. 2012; 51:114–122. [PubMed: 22561877]
21. Burr DB, Martin RB, Schaffler MB, Radin EL. Bone remodeling in response to in vivo fatigue microdamage. J Biomech. 1985; 18:189–200. [PubMed: 3997903]
22. Lee TC, Staines A, Taylor D. Bone adaptation to load: Microdamage as a stimulus for bone remodelling. J Anat. 2002; 201:437–446. [PubMed: 12489756]
23. Abrahamsen B, Eiken P, Eastell R. Subtrochanteric and diaphyseal femur fractures in patients treated with alendronate: A register-based national cohort study. J Bone Miner Res. 2009; 24:1095–1102. [PubMed: 19113931]
24. Lenart BA, Lorich DG, Lane JM. Atypical fractures of the femoral diaphysis in postmenopausal women taking alendronate. N Engl J Med. 2008; 358:1304–1306. [PubMed: 18354114]
25. Lenart BA, Neviaser AS, Lyman S, Chang CC, Edobor-Osula F, Steele B, van der Meulen MC, Lorich DG, Lane JM. Association of low-energy femoral fractures with prolonged bisphosphonate use: A case control study. Osteoporos Int. 2009; 20:1353–1362. [PubMed: 19066707]
26. Neviaser AS, Lane JM, Lenart BA, Edobor-Osula F, Lorich DG. Low-energy femoral shaft fractures associated with alendronate use. J Orthop Trauma. 2008; 22:346–350. [PubMed: 18448990]
27. Park-Wyllie LY, Mamdani MM, Juurlink DN, Hawker GA, Gunraj N, Austin PC, Whelan DB, Weiler PJ, Laupacis A. Bisphosphonate use and the risk of subtrochanteric or femoral shaft fractures in older women. JAMA. 2011; 305:783–789. [PubMed: 21343577]
28. Shane E, Burr D, Ebeling PR, Abrahamsen B, Adler RA, Brown TD, Cheung AM, Cosman F, Curtis JR, Dell R, Dempster D, Einhorn TA, Genant HK, Geusens P, Klaushofer K, Koval K, Lane JM, McKiernan F, McKinney R, Ng A, Nieves J, O'Keefe R, Papapoulos S, Sen HT, van der Meulen MC, Weinstein RS, Whyte M. Atypical subtrochanteric and diaphyseal femoral fractures: Report of a task force of the American Society for Bone and Mineral Research. J Bone Miner Res. 2010; 25:2267–2294. [PubMed: 20842676]

29. Somford MP, Draijer FW, Thomassen BJW, Chavassieux PM, Boivin G, Papapoulos SE. Bilateral fractures of the femur diaphysis in a patient with rheumatoid arthritis on long-term treatment with alendronate: Clues to the mechanism of increased bone fragility. J Bone Miner Res. 2009; 24:1736–1740. [PubMed: 19419297]
30. Dell RM, Adams AL, Greene DF, Funahashi TT, Silverman SL, Eisemon EO, Zhou H, Burchette RJ, Ott SM. Incidence of atypical nontraumatic diaphyseal fractures of the femur. J Bone Miner Res. 2012; 27:2544–2550. [PubMed: 22836783]
31. Burr DB, Turner CH, Naick P, Forwood MR, Ambrosius W, Hasan MS, Pidaparti R. Does microdamage accumulation affect the mechanical properties of bone? J Biomech. 1998; 31:337–345. [PubMed: 9672087]
32. Carter DR, Hayes WC, Schurman DJ. Fatigue life of compact bone--II. Effects of microstructure and density. J Biomech. 1976; 9:211–218. [PubMed: 1262355]
33. Hoshaw SJ, Cody DD, Saad AM, Fyhrie DP. Decrease in canine proximal femoral ultimate strength and stiffness due to fatigue damage. J Biomech. 1997; 30:323–329. [PubMed: 9074999]
34. Pattin CA, Caler WE, Carter DR. Cyclic mechanical property degradation during fatigue loading of cortical bone. J Biomech. 1996; 29:69–79. [PubMed: 8839019]
35. Schaffler MB, Radin EL, Burr DB. Long-term fatigue behavior of compact bone at low strain magnitude and rate. Bone. 1990; 11:321–326. [PubMed: 2252810]
36. Landrigan MD, Roeder RK. Systematic error in mechanical measures of damage during four-point bending fatigue of cortical bone. J Biomech. 2009; 42:1212–1217. [PubMed: 19394019]
37. Boyce TM, Fyhrie DP, Glotkowski MC, Radin EL, Schaffler MB. Damage type and strain mode associations in human compact bone bending fatigue. J Ortho Res. 1998; 16:322–329.
38. Dempster DW, Compston JE, Drezner MK, Glorieux FH, Kanis JA, Malluche H, Meunier PJ, Ott SM, Recker RR, Parfitt AM. Standardized nomenclature, symbols, and units for bone histomorphometry: A 2012 update of the report of the ASBMR histomorphometry nomenclature committee. J Bone Miner Res. 2013; 28:2–17. [PubMed: 23197339]
39. Scholz FW, Stephens MA. K-sample anderson-darling tests. J American Statistical Association. 1987; 82:918–924.
40. Diab T, Vashishth D. Effects of damage morphology on cortical bone fragility. Bone. 2005; 37:96–102. [PubMed: 15897021]
41. Tjhia CK, Odvina CV, Sudhaker RD, Stover SM, Wang X, Fyhrie DP. Mechanical property and tissue mineral density differences among severely suppressed bone turnover (SSBT) patients, osteoporotic patients, and normal subjects. Bone. 2011; 49:1279–1289. [PubMed: 21958843]
42. Frost HM. Human haversian system measurements. Henry Ford Hosp Med Bull. 1961; 9:145–147. [PubMed: 13702275]
43. Jaworski ZF. Lamellar bone turnover system and its effector organ. Calcif Tissue Int. 1984; 36(S1):S46–S55. [PubMed: 6430522]
44. Burr DB, Schaffler MB, Frederickson RG. Composition of the cement line and its possible mechanical role as a local interface in human compact bone. J Biomech. 1988; 21:939–945. [PubMed: 3253280]
45. Koester KJ, Ager JW, Ritchie RO. The true toughness of human cortical bone measured with realistically short cracks. Nat Mater. 2008; 7:672–677. [PubMed: 18587403]
46. Lakes R, Saha S. Cement line motion in bone. Science. 1979; 204:501–503. [PubMed: 432653]
47. Qiu S, Rao DS, Palnitkar S, Parfitt AM. Dependence of bone yield (volume of bone formed per unit of cement surface area) on resorption cavity size during osteonal remodeling in human rib: Implications for osteoblast function and the pathogenesis of age-related bone loss. J Bone Miner Res. 2010; 25:423–430. [PubMed: 19821766]
48. Qiu S, Rao DS, Palnitkar S, Parfitt AM. Reduced iliac cancellous osteocyte density in patients with osteoporotic vertebral fracture. J Bone Miner Res. 2003; 18:1657–1663. [PubMed: 12968675]
49. Schaffler MB, Choi K, Milgrom C. Aging and matrix microdamage accumulation in human compact bone. Bone. 1995; 17:521–525. [PubMed: 8835305]
50. Norman TL, Wang Z. Microdamage of human cortical bone: Incidence and morphology in long bones. Bone. 1997; 20:375–379. [PubMed: 9108359]

51. Ruppel ME, Burr DB, Miller LM. Chemical makeup of microdamaged bone differs from undamaged bone. Bone. 2006; 39(2):318–324. [PubMed: 16584933]
52. Poundarik AA, Diab T, Sroga GE, Ural A, Boskey AL, Gundberg CM, Vashishth D. Dilatational band formation in bone. Proc Natl Acad Sci USA. 2012; 109:19178–19183. [PubMed: 23129653]
53. Allen MR, Burr DB. Bisphosphonate effects on bone turnover, microdamage, and mechanical properties: What we think we know and what we know that we don't know. Bone. 2011; 49:56–65. [PubMed: 20955825]
54. Allen MR, Erickson AM, Wang X, Burr DB, Martin RB, Hazelwood SJ. Morphological assessment of basic multicellular unit resorption parameters in dogs shows additional mechanisms of bisphosphonate effects on bone. Calcif Tissue Int. 2010; 86:67–71. [PubMed: 19953232]
55. Boyce RW, Paddock CL, Gleason JR, Sletsema WK, Eriksen EF. The effects of risedronate on canine cancellous bone remodeling: Three-dimensional kinetic reconstruction of the remodeling site. J Bone Miner Res. 1995; 10:211–221. [PubMed: 7754801]
56. Eriksen EF. Cellular mechanisms of bone remodeling. Rev Endocr Metab Disord. 2010; 11:219–227. [PubMed: 21188536]
57. Jowsey J. Studies of haversian systems in man and some animals. J Anat. 1966; 100:857–864. [PubMed: 4961449]

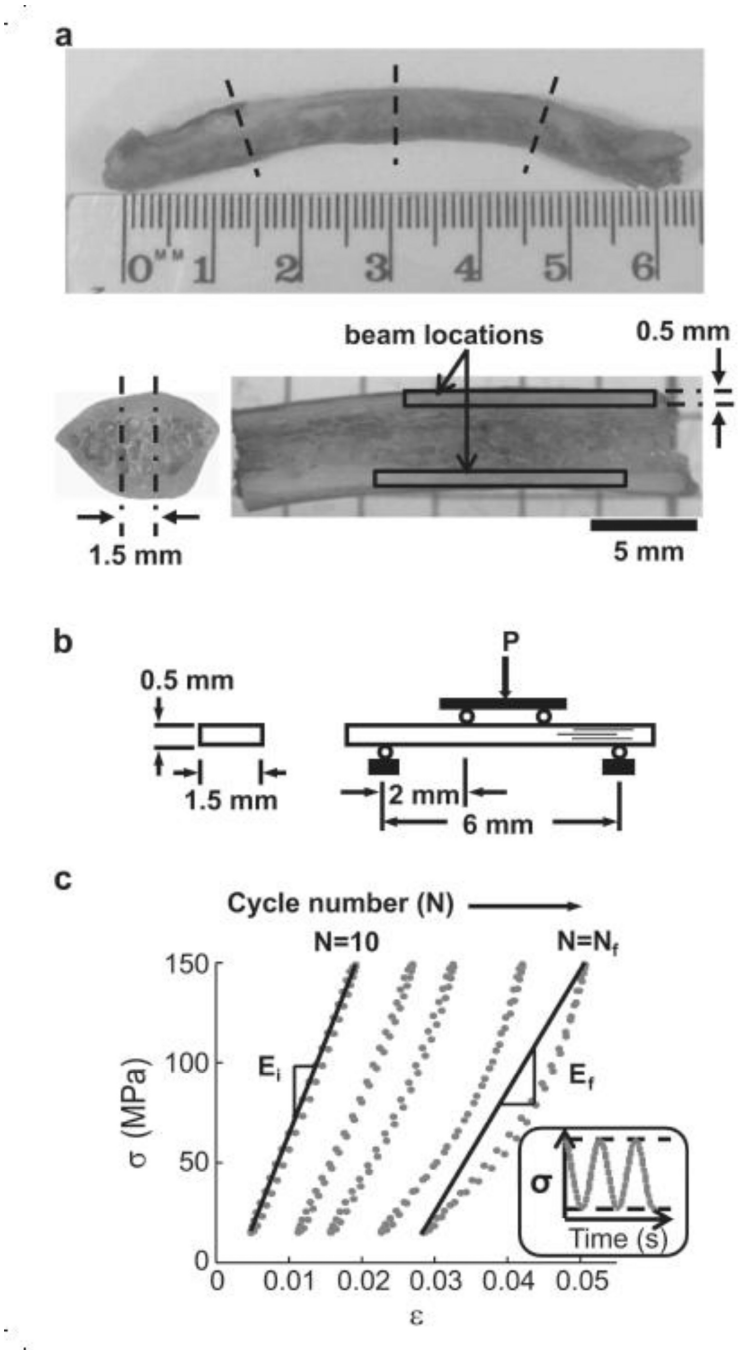


**Figure 1.**

Mechanical fatigue testing. (a) Location of cuts for cortical bone beams prepared from 11th rib highlighted by dotted lines. Outlines show possible locations for primary and final beam sections made along the medio-lateral axis. (b) Beam specimen geometry and 4-point bending set-up. Load (P) was directed downward at the top load points. Lines within beam indicate osteonal orientation. (c) Stress ($\sigma_a$) versus strain ($\varepsilon$) hysteresis for sinusoidal loading of a single bone beam within a predetermined maximum and minimum stress (inset). Five representative load cycles out of thousands are plotted. The slope of the line is the modulus

(E) at the initial ($N_i$) and final ($N_f$) full cycles. $N_i$ represents the $10^{th}$ cycle, and $N_f$ the cycle just prior to the partial cycle upon which failure occurred.

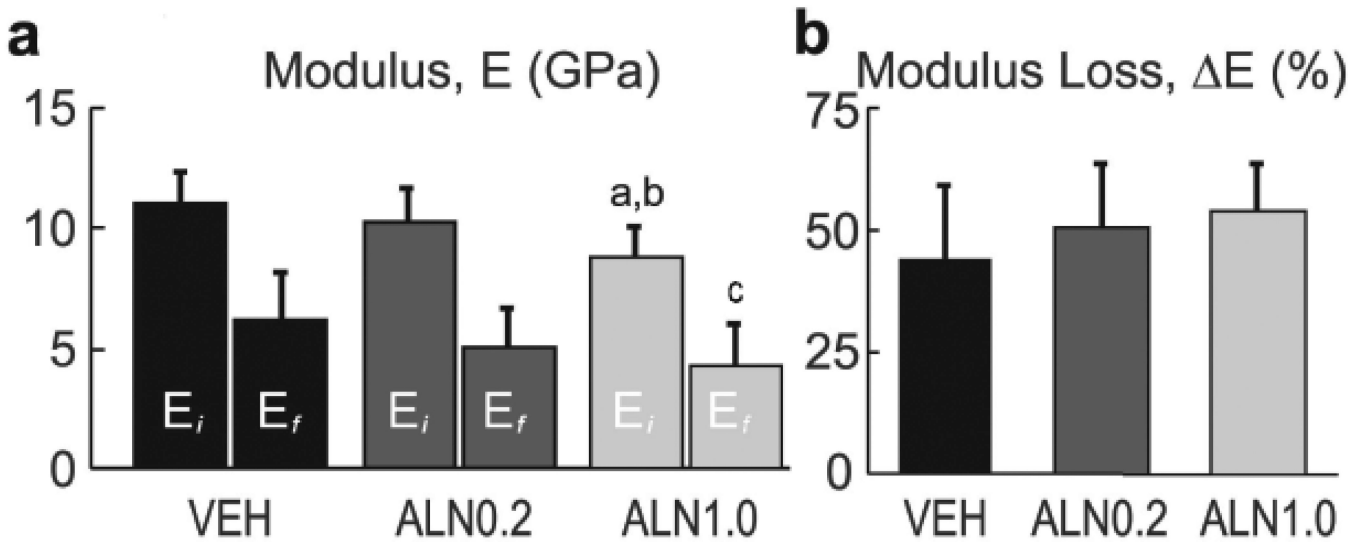


**Figure 2.**

Modulus and modulus loss. (a) Average initial modulus ($E_i$), final modulus ($E_f$) and (b) normalized reduction in modulus ($\Delta E/E_i = 100\% - E_f/E_i$). Means ± SD; n = 7 – 10 / group. Analysis by ANOVA, followed by Tukey HSD. $E_i$: **a** vs. ALN0.2 ($p<0.01$), **b** vs. VEH control ($p < 0.001$). $E_f$: **c** vs. VEH ($p<0.01$).

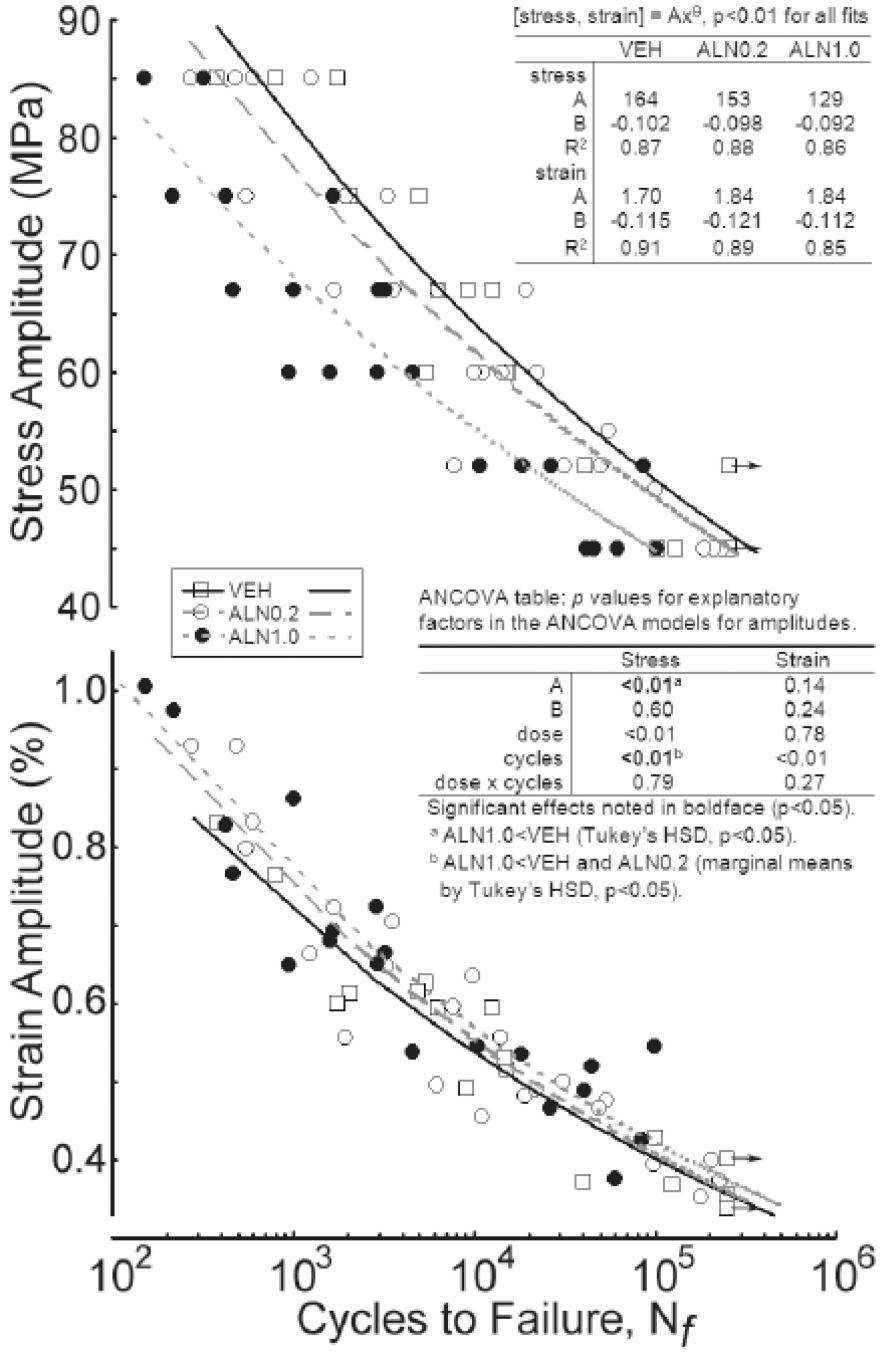


**Figure 3.**

Fatigue-life diagrams for bone beams cyclically tested under 4-point bending at 6 stress amplitudes ($\sigma_a$). Each point represents the number of cycles to failure ($N_f$) plotted on a log scale vs. $\sigma_a$ and apparent strain ($\varepsilon$) amplitude for each beam tested at one randomly predetermined $\sigma_a$. Failure was defined by either fracture of beam or a 2.5 mm total deflection, whichever occurred first (see 2.2). Medial beams from 2 VEH-treated beagles had not failed at $N_f$ = 250,000 cycles (indicated by arrows). Each line represents a power law fit for the mean fatigue response of each treated group with the equations indicated

($p<0.01$ by linear regression). ANCOVA (table insert), followed by Tukey HSD indicated >3-fold fewer cycles to failure for ALN1.0 versus VEH under the stress amplitudes applied. No differences exist in models adjusted to apparent strain amplitude.

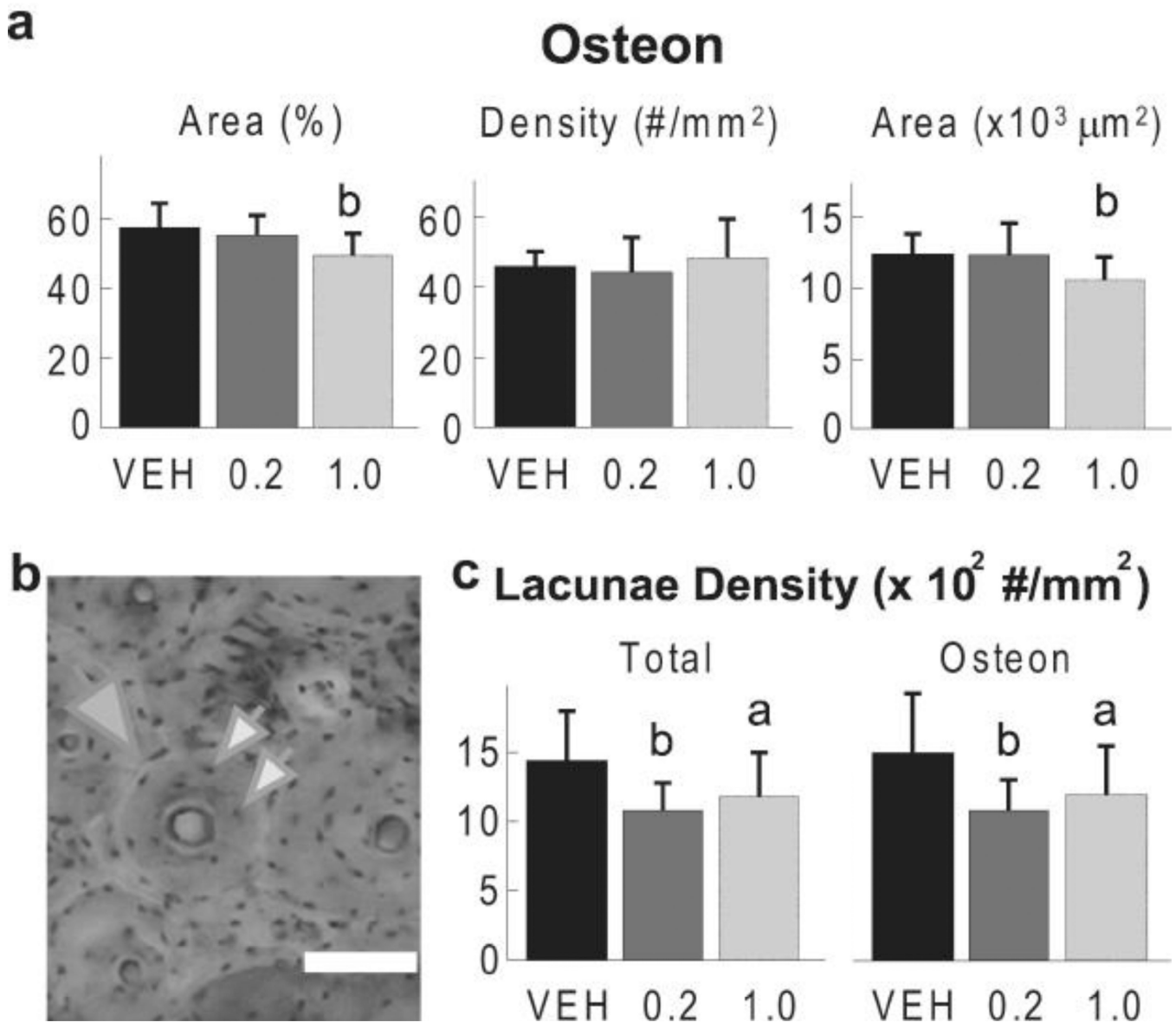


**Figure 4.**

ALN-induced differences in average osteon size and lacunae density. (a) Cross sectional area contained in osteons normalized by beam area, osteon density (On.Dn) and average area of osteons (On.Ar) for beams in each of the 3 groups. (b) Section of one beam cross-section illustrating osteons (large arrow) and osteocyte lacunae (smaller arrows); scale bar = 100 µm. (c) Total and osteon osteocyte lacunae areal density (Ot.Lc.Dn). Means ± SD; n = 7 – 10 / group. ANOVA, followed by Tukey HSD: vs. control (VEH), [a] $p<0.05$, [b] $p < 0.01$

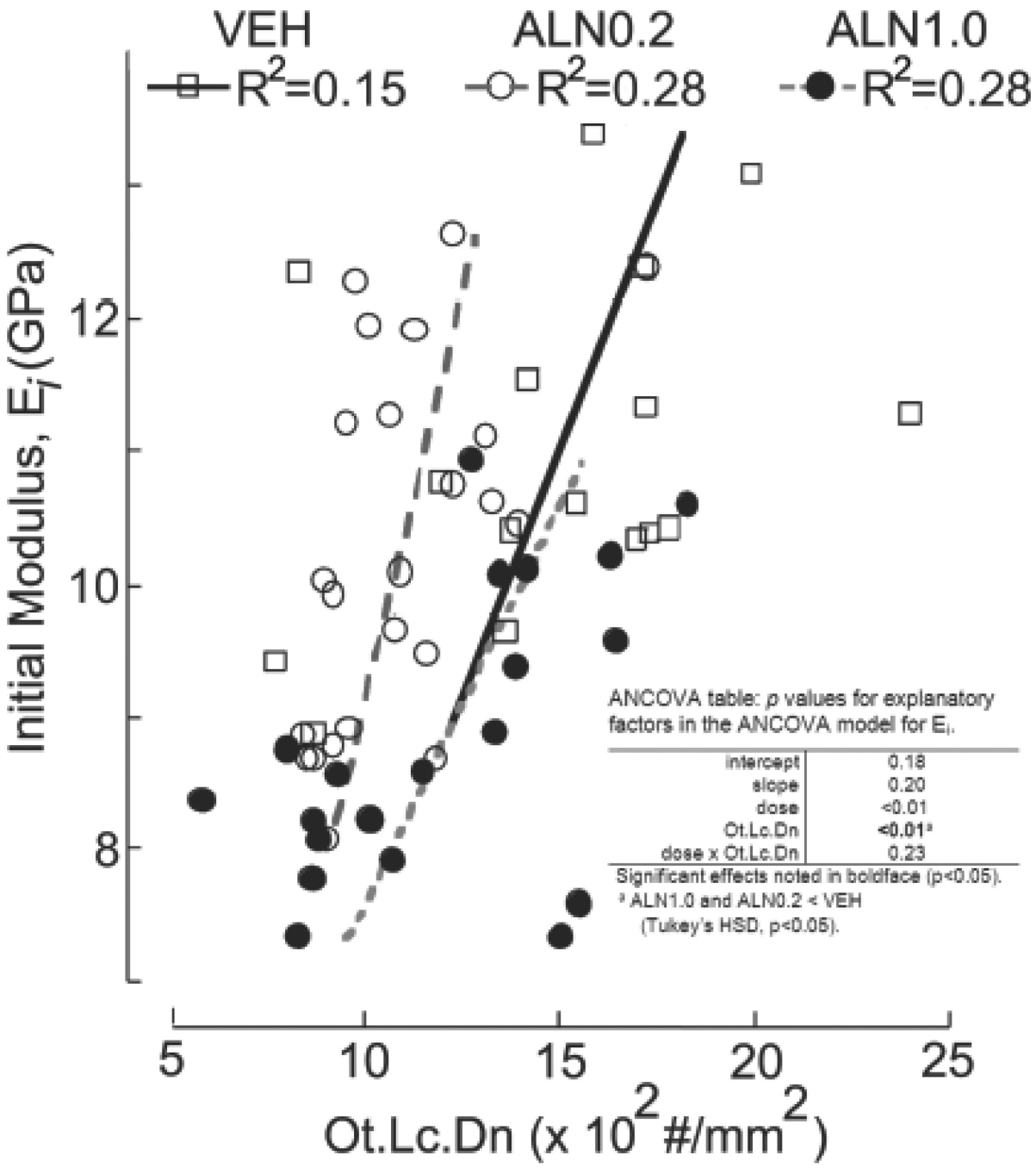


**Figure 5.**

Relationship between initial beam stiffness ($E_i$) and osteocyte lacunar density (Ot.Lc.Dn). $E_i$ was moderately and positively correlated with Ot.Lc.Dn for all groups by ANCOVA (table insert), followed by Tukey HSD ($p<0.01$). No differences, beyond the previously demonstrated differences in $E_i$ means, were found ($p>0.15$).

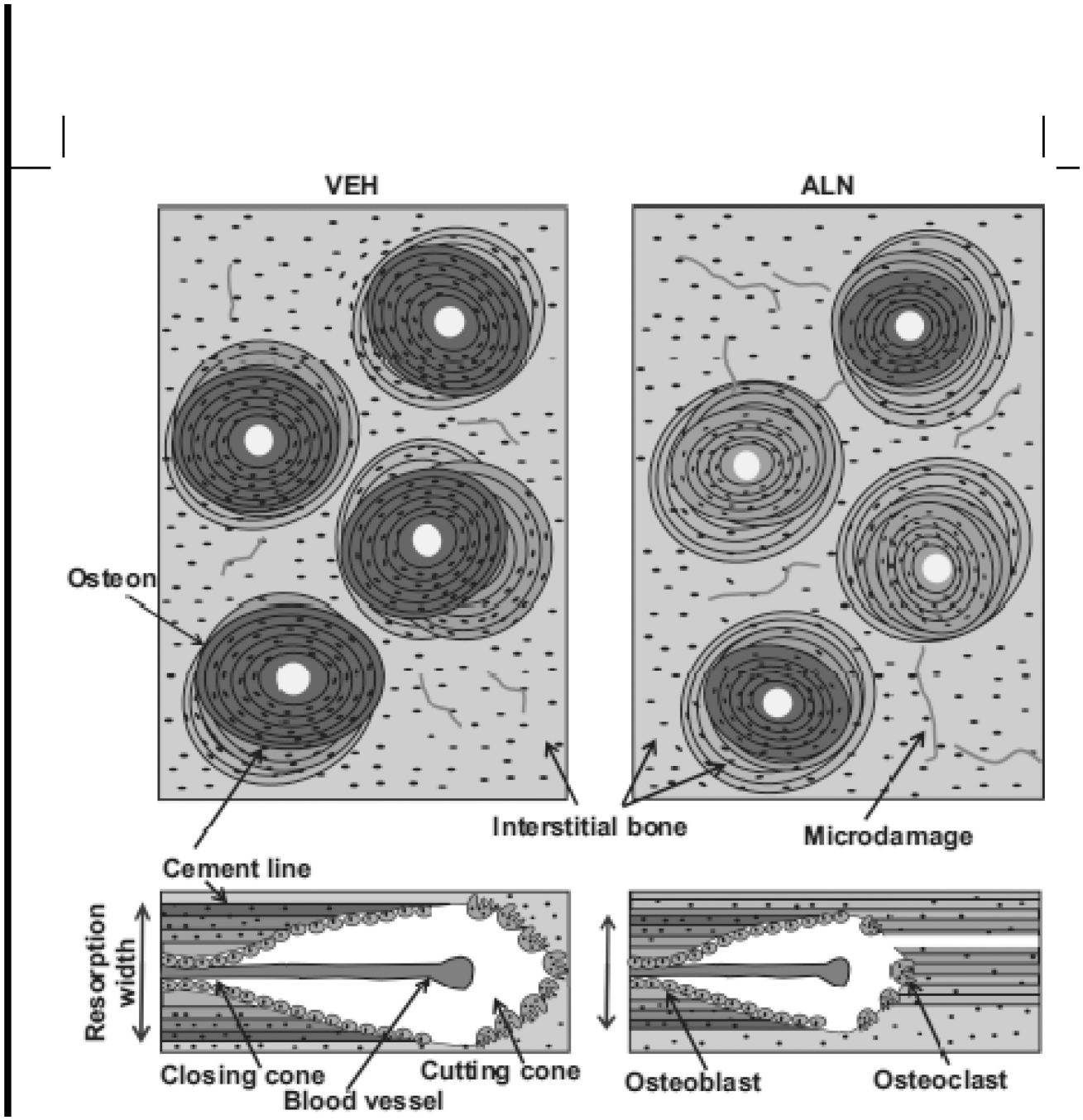


**Figure 6.**

Model for the observations of decreased osteonal size and increased micro-crack length in long-term ALN-treated cortical bone tissue. Decreases in the resorption width dug by the osteoclasts of basic multicellular units (BMUs) decrease the average osteon area and total cement line perimeter, and increase the interstitial area where most micro-cracks initiate and lengthen. Interstitial (lightest gray) cortical bone is older than osteonal bone. Additionally, because activation frequency for new BMUs is lower with ALN, the newest of osteons (darkest gray) may be fewer in number and older on average. The reduced cement line

perimeter further reduces the tough, energy-absorbing interfaces available for slowing crack growth and accumulation. These losses in energy-absorbing capacity can lead to a significant reduction in tissue stiffness and number of cycles to failure as measured in this study.

## Table 1

Cortical bone traits, as measured by X-ray micro-computed tomography of ribs (n=6/group).

| | VEH | ALN0.2 | ALN1.0 |
|---|---|---|---|
| Ct.Wi (μm) | 470±41 | 483±45 | 514±61 |
| Ct.Ar ($mm^2$) | 7.43±0.60 | 7.41±0.77 | 7.42±0.98 |
| Ma.Ar ($mm^2$) | 6.42±0.93 | 5.14±0.80[a] | 4.84±1.21[a] |
| Ct.Ar/Tt.Ar (%) | 53.8±3.9 | 58.7±3.5[a] | 60.8±5.7[a] |
| Ct.TMD ($g/cm^3$) | 1.16±0.04 | 1.16±0.03 | 1.15±0.06 |

Data represented as mean ± SD were analyzed by ANOVA followed by Tukey HSD: vs. control (VEH)

[a] $p<0.05$.

## Table 2

Cortical bone osteonal canal area (Ca.Ar) traits, as measured by morphometry of beams.

| | VEH (n=9) | ALN0.2 (n=7) | ALN1.0 (n=10) |
|---|---|---|---|
| Ca.Ar (%) | 2.02±0.52 | 2.40±0.50 | 2.32±0.63 |
| Ca.Ar ($\mu m^2$) | 383±113 | 500±146 | 451±171 |

The first value is normalized by beam cross-sectional area and is equivalent to porosity, and the second is an average for canal size. Data represented as mean ± SD. No differences by ANOVA comparisons between doses ($p>0.15$, n.s.).